

Effects of W^{6+} occupying Sc^{3+} on the structure, vibration, and thermal expansion properties of scandium tungstate

Dongxia Chen(陈冬霞), Qiang Sun(孙强), Zhanjun Yu(于占军), Mingyu Li(李明玉), Juan Guo(郭娟), Mingju Chao(晁明举), and Erjun Liang(梁二军)

Citation: Chin. Phys. B, 2021, 30 (**6**): 066501. DOI: 10.1088/1674-1056/abd7d4
Journal homepage: http://cpb.iphy.ac.cn; http://iopscience.iop.org/cpb

What follows is a list of articles you may be interested in

Low thermal expansion and broad band photoluminescence of $Zr_{0.1}Al_{1.9}Mo_{2.9}V_{0.1}O_{12}$

Jun-Ping Wang(王俊平), Qing-Dong Chen(陈庆东), Li-Gang Chen(陈立刚), Yan-Jun Ji(纪延俊), You-Wen Liu(刘友文), and Er-Jun Liang(梁二军)

Chin. Phys. B, 2021, 30 (**3**): 036501. DOI: 10.1088/1674-1056/abcf39

Lattice thermal conductivity of β_{12} and χ_3 borophene

Jia He(何佳), Yulou Ouyang(欧阳宇楼), Cuiqian Yu(俞崔前), Pengfei Jiang(蒋鹏飞), Weijun Ren(任卫君), and Jie Chen(陈杰)

Chin. Phys. B, 2020, 29 (**12**): 126503. DOI: 10.1088/1674-1056/abbbe6

Tuning thermal transport via phonon localization in nanostructures

Dengke Ma(马登科), Xiuling Li(李秀玲), and Lifa Zhang(张力发)

Chin. Phys. B, 2020, 29 (**12**): 126502. DOI: 10.1088/1674-1056/abb7fa

Charge structure factors of doped armchair nanotubes in the presence of electron-phonon interaction

Hamed Rezania, Farshad Azizi

Chin. Phys. B, 2020, 29 (**9**): 096501. DOI: 10.1088/1674-1056/ab942e

Negative thermal expansion of Ca_2RuO_4 with oxygen vacancies

Sen Xu(徐森), Yangming Hu(胡杨明), Yuan Liang(梁源), Chenfei Shi(史晨飞), Yuling Su(苏玉玲), Juan Guo(郭娟), Qilong Gao(高其龙), Mingju Chao(晁明举), Erjun Liang(梁二军)

Chin. Phys. B, 2020, 29 (**8**): 086501. DOI: 10.1088/1674-1056/ab8a36

Effects of W^{6+} occupying Sc^{3+} on the structure, vibration, and thermal expansion properties of scandium tungstate*

Dongxia Chen(陈冬霞)[1], Qiang Sun(孙强)[2], Zhanjun Yu(于占军)[1], Mingyu Li(李明玉)[1], Juan Guo(郭娟)[2], Mingju Chao(晁明举)[2], and Erjun Liang(梁二军)[2,†]

[1] *School of Materials Science & Engineering, Zhengzhou University of Aeronautics, Zhengzhou* 450046, *China*
[2] *Key Laboratory of Materials Physics of Ministry of Education, School of Physics and Microelectronics, Zhengzhou University, Zhengzhou* 450052, *China*

(Received 14 December 2020; revised manuscript received 30 December 2020; accepted manuscript online 4 January 2021)

We experimentally investigate effects of W^{6+} occupying the sites of Sc^{3+} in the unit cell of $Sc_2W_3O_{12}$ ($Sc_8W_{12}O_{48}$) on the structure, vibration and thermal expansion. The composition and structure of the doped sample $(Sc_6W_2)W_{12}O_{48\pm\delta}$ (with two W^{6+} occupying two sites of Sc^{3+} in the unit cell of $Sc_8W_{12}O_{48}$) are analyzed and identified by combining the x-ray photoelectron spectroscopy and the synchronous x-ray diffraction with first-principles calculations based on density functional theory. Results show that the crystal with even W^{6+} occupying even Sc^{3+} in the unit cell is stable and maintains the orthorhombic structure at room temperature. The structure of the doped sample is similar to that of $Sc_2W_3O_{12}$, and with even W occupying even positions of Sc in the unit cell and constituting the WO_6 octahedra. Raman analyses show that the doped sample possesses stronger W–O bonds and wider Raman linewidths than those of $Sc_2W_3O_{12}$. The sample doped with W also exhibits intrinsic negative thermal expansion in the measured range of 150 K–650 K.

Keywords: structure, negative thermal expansion, Raman spectroscopy

PACS: 65.40.De, 61.66.–f, 71.30.+h **DOI:** 10.1088/1674-1056/abd7d4

1. Introduction

Materials with negative thermal expansion (NTE) property have potential applications in many fields such as precision optics, optoelectronic devices, and aerospace materials. Usually, NTE materials can be compounded with positive thermal expansion materials or tailored chemically to attain near zero or controllable thermal expansion materials. Such materials are especially suitable for use in heat cycles due to the low mismatch or less thermal stress. AW_2O_8[1] and AV_2O_7 (A = Zr, Hf)[2,3] are two types of well-known framework NTE oxides which possess isotropic NTE property and wide temperature ranges of NTE. A number of studies have shown that AW_2O_8 is metastable at high temperature, while AV_2O_7 undergoes a structure phase transition at about 427 K. Materials with general formula of $A_2M_3O_{12}$ (A = +3 ions; M = Mo, W) also exhibit NTE properties in a wide temperature range but NTE is anisotropic. Except for $Sc_2W_3O_{12}$,[4,5] all the members of $A_2M_3O_{12}$ family show either structure phase transition (e.g., $Fe_2Mo_3O_{12}$, $Cr_2Mo_3O_{12}$, $Al_2Mo_3O_{12}$,[6] $Al_2W_3O_{12}$ and $In_2W_3O_{12}$)[7] or hydroscopicity (e.g., $Yb_2Mo_3O_{12}$,[8] $Y_2Mo_3O_{12}$[9] and $Y_2W_3O_{12}$).[10] A great deal of research has been carried out to control the phase transition or hydroscopicity of $A_2M_3O_{12}$ by substituting A^{4+} or M^{6+} with other ions.[11–19] In addition, $PbTiO_3$ based ferroelectric transition materials,[20–22] Mn_3AN based materials with magnet volume effect[23–25] and $TaVO_5$[26] also exhibit NTE properties.

Recent years, tetra-molybdates with NTE properties in a narrow region have been reported, e.g., $Ln_2Mo_4O_{15}$ (Ln = Y, Dy, Ho, Tm),[27] $Ce_2(MoO_4)_2(Mo_2O_7)$,[28] and $R_2Mo_4O_{15}$ (R = La, Nd, Sm).[29] It is worth noting that all of these materials adopt monoclinic structure, of which, two $Mo(2)O_4$ tetrahedra are connected by a bridge O atom to form a pyromolybdate $Mo(2)_2O_7$ group that is similar to V_2O_7 group in ZrV_2O_7. One $Mo(2)_2O_7$ polyhedron is weakly joined with two $Mo(1)O_4$ tetrahedra by sharing O atoms to form an entire Mo_4O_{15} group. Each +3 metal atom is coordinated with seven oxygen atoms to constitute a single capped trigonal prism.

Meanwhile, $Cu_2P_2O_7$ has been found to exhibit the strongest NTE among the oxides ($\alpha_v \sim -27.69 \times 10^{-6}$ K^{-1}, 5 K–375 K).[30] The NTE behaviors of Prussian blue analogues, e.g., $FeFe(CN)_6$,[31] $M^{II}_2M^{IV}(CN)_8$ (M^{II} = Ni, Co, Fe, and Mn; M^{IV} = Mo and W),[32] $ScCo(CN)_6$[33] and YFe(CN)6[34] were also reported in recent years.

In this paper, a new tungstate $(Sc_6W_2)W_{12}O_{48\pm\delta}$ with the structure similar to the orthorhombic structure of $Sc_2W_3O_{12}$ is studied by two W^{6+} occupying two sites of Sc^{3+} in the unit cell of $Sc_2W_3O_{12}$. The structure, vibration and thermal ex-

*Project supported by the National Science Foundation of China (Grant Nos. 11574276 and 11874328), the Key Scientific Research Project of Universities in Henan Province (Grant Nos. 20B140018, 20A510012, and 19A140019), Key Scientific and Technological Project of Henan Province (Grant Nos. 202102210110, 182102210451 and 192102210002). The use of the Advanced Photon Source at Argonne National Laboratory was supported by the U.S. Department of Energy, Office of Science, Office of Basic Energy Sciences (Grant No. DE-AC02-06CH11357).

†Corresponding author. E-mail: ejliang@zzu.edu.cn

© 2021 Chinese Physical Society and IOP Publishing Ltd

pansion properties of the doped sample are investigated experimentally. The results of Rietveld refinement of synchronous x-ray diffraction (SXRD) data indicate that the structure of the doped sample is similar to that of orthorhombic $Sc_2W_3O_{12}$. Blue shifts of peak positions and increasement of FWHMs are found in the spectrum of the doped sample by comparing the Raman spectrum with that of $Sc_2W_3O_{12}$. The distortion of polyhedra and stress introduced by W^{6+} occupying Sc^{3+} in the unit cell are attributed to those changes. In order to demonstrate this structure of the doped sample, the effects of odd/even W^{6+} occupying the odd/even sites of Sc^{3+} in the unit cell on the stability of crystal are studied by first-principles calculations based on DFT. It is shown that the structure by odd W^{6+} occupying odd Sc^{3+} in the unit cell is unstable because of the severe distortion of the unit cell, while it is stable by even W^{6+} occupying even Sc^{3+} in the unit cell. Simultaneously, according to the changes of cell parameters with temperature, an intrinsic NTE property is discovered in the doped sample.

2. Experimental procedure and computational details

The sample of $(Sc_6W_2)W_{12}O_{48\pm\delta}$ was synthesized by a solid-state reaction method. Commercial chemicals Sc_2O_3 and WO_3 (99.9% purity) were used as the starting materials. The materials were weight according to the stoichiometric ratios, then mixed and ground in a mortar for 2 h. The obtained uniform powders were transferred to a corundum ark and heated in a tube furnace of 1753 K for 5 min, then rapidly quenched in deionized water and placed in of about 400 K for 0.5 h. Repeat the above procedure, the sample was sintered for a second time at 1753 K for 1 h. To ensure the purity, the sample was sintered for a third time at 1753 K for 30 min and then cooled out. The sintered powders were reground, pressed into pellets then sintered again at 1173 K for 30 min.

X-ray photoelectron spectrometer (XPS) (Axis Ultra, Kratos, UK) was used to analyze the composition of the doped sample and the valence of the elements. The casaXPS (version 2.3.16) software was used to process the data. Crystal structure and CTEs of the sample were determined by synchrotron x-ray diffraction (SXRD). Temperature-dependent SXRD data were collected by an instrument 11-ID-C at the Advanced Photon Source with a wavelength of 0.11730 Å. The structure together with lattice constants was refined using an orthorhombic structural model (space group: *Pbcn*). All the calculations of structure and lattice constants were performed on Fullprof software (version 1.10). Raman spectra were recorded by a LabRAM HR Evolution Raman spectrometer (France HORIBA Jobin Yvon S.A.S.) with the excitation wavelength of 532 nm.

To predict the stable structure of the doped system, the first-principles calculations based on DFT were performed as implemented in the Vienna *ab initio* simulation package (VASP).[35] The ion–electron interaction is depicted by projector augmented wave (PAW) method,[36] and the exchange and correlation effects are described by the GGA-PBE functional.[37] The wave functions are expanded by the plane waves up to an energy cutoff of 380 eV. Due to the large unit cell ($\sim$10 Å $\times$ 10 Å $\times$ 13 Å), integrals over the first BZ are approximated by a Monkhorst–Pack K-point mesh of $1 \times 1 \times 1$. The total energy was calculated with high precision, converged to 10^{-7} eV/atom, and the structural relaxation was stopped when the residual forces become less than 10^{-3} eV/Å.

The substitutional energy of Sc replaced by W is calculated by

$$E_{\text{sub}} = E_{\text{doped}} + nE_{\text{Sc(atom)}} - \left(E_{\text{undoped}} + nE_{\text{W(atom)}}\right),$$

where E_{sub} is substitutional energy, E_{doped} and E_{undoped} are the total energy of W doped and undoped systems, respectively; $E_{\text{Sc(atom)}}$ and $E_{\text{W(atom)}}$ are energy of per Sc or W atom; n is the number of substitutional W.

3. Results and discussion

Figure 1(a) shows the XPS total spectrum of the doped sample. It can be seen that the spectrum contains the elements of C, Sc, W and O. The C element is derived from the experimental oil pump. Figures 1(b)–1(d) give the XPS spectra of Sc 2p, W 4f and O 1s. The integrated areas of the XPS peaks were calculated to determine the atomic ratio of the sample. Lorenz fittings of the peaks were used to determine the binding energies of Sc 2p, W 4f and O 1s and then the valence of element. The spin-orbit splitting of Sc 2p into $2p_{3/2}$ and $2p_{1/2}$ were found in the Sc 2p spectrum. The corresponding binding energies are 402.67 eV and 407.26 eV, respectively. The W 4f spectrum (Fig. 1(c)) can be fitted by two Lorenz peaks with the binding energies of 35.37 eV and 37.63 eV for W $4f_{7/2}$ and W $4f_{5/2}$, respectively. It indicates that the tungsten ions in the sample are in +6 valence. By fitting the spectrum of O 1s (Fig. 1(d)), the binding energies were found to be 530.53 eV and 531.82 eV. Table 1 gives the semi-quantitative results of the XPS spectra. It can be seen that the atomic ratio of the sample is $Sc : W : O \approx 1 : 2.50 : 9.68$, which is very close to the design ratio of $6 : 14 : 48 \pm \delta$.

Table 1. The integration results of the XPS peaks and the atomic ratio of Sc 2p, W 4f and O 1s.

Element	RSF	Area	Area/RSF	Atomic ratio (%)
Sc 2p	6.38	8100.6	1269.7	7.59
W 4f	9.80	31051.5	3168.5	18.95
O 1s	2.93	35998.9	12286.2	73.46

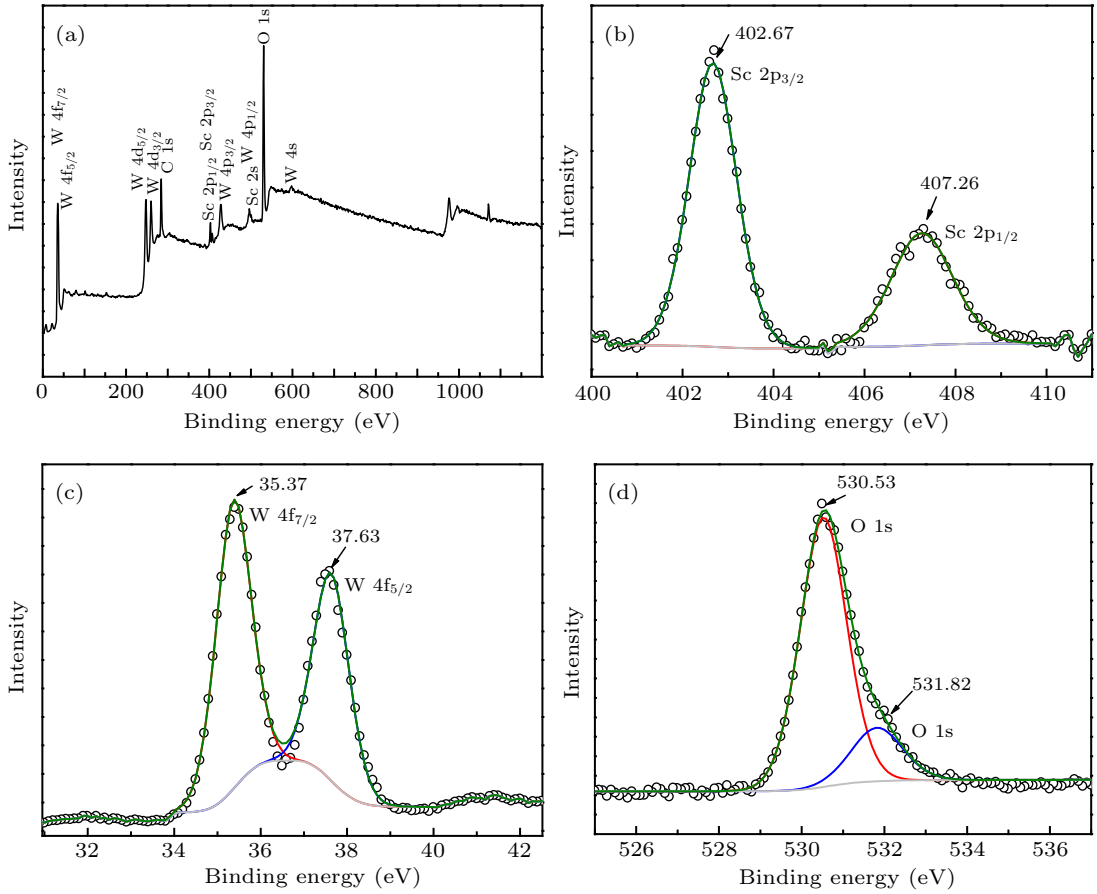


Fig. 1. XPS spectra of the doped sample: (a) total XPS spectrum; (b)–(d) XPS spectra corresponding to the Sc 2p, W 4f, and O 1s.

Figure 2(a) gives the Rietveld refined results of the XRD spectrum at 300 K for the doped sample (the black curve as the measured intensity; the red symbol as the calculated intensity). The results show that the sample adopts an orthorhombic structure at room temperature with space group *Pbcn* (No. 60). The lattice constants obtained by the refinement are as follows: $a = 13.2461(6)$ Å, $b = 9.52801(5)$ Å, $c = 9.6208(5)$ Å, $V = 1214.2(1)$ Å^3. The reliability factors for the refinement are as follows: $R_p = 11.4$, $R_{wp} = 13.9$ and $R_{exp} = 1.61$. The cell parameters of the basic material $Sc_2W_3O_{12}$ at room temperature (300 K) reported previously[38] are as below: $a = 9.6720$ Å, $b = 13.318$ Å, $c = 9.5795$ Å, $V = 1234.0$ Å^3. Comparing the two sets of data, it is not difficult to find that the cell parameters of the doped sample are slightly smaller than those of $Sc_2W_3O_{12}$. Figure 2(b) shows a partial enlargement of the XRD pattern of the sample at 300 K. Each peak in the figure can be well indexed. Table 2 provides the metal coordinates and atomic occupancies of the doped sample and $Sc_2W_3O_{12}$. As can be seen from the table, it contains three unequivalent positions of W in the unit cell of the doped sample, where $\sim 16\%$ of the Sc positions are occupied by W. Figure 2(c) presents the structure schematic diagram of the doped sample by the Rietveld refinement. The framework of the crystal consists of corner-shared WO_4 tetrahedra and ScO_6/WO_6 octahedra. There are four W(1)O_4 tetrahedra and eight W(2)O_4 tetrahedra occupying the normal lattice positions similar to $Sc_2W_3O_{12}$. The additional W(3) occupies the positions of Sc and forms WO_6 octahedra. Each ScO_6/WO_6 octahedron shares its six oxygen atoms with the adjacent WO_4 tetrahedra, and each WO_4 tetrahedron shares all of its oxygen atoms with the adjacent ScO_6 octahedra. Therefore, the structure can be regarded as quasi-rigid unit modules (QRUMs). It can be concluded that the synthesized sample crystallizes into an orthorhombic structure similar to that of $Sc_2W_3O_{12}$, and with two W^{6+} occupying two sites of Sc^{3+} in the unit cell of $Sc_2W_3O_{12}$.

Figure 2(d) gives the temperature-dependent SXRD patterns of the doped sample. As temperature increasing, no significant change was observed in the patterns, indicating that no phase transition occurs within 150–650 K. Also, there are no impurity peaks in the patterns other than the XRD peaks of the orthorhombic structure, indicating that the sample is a pure single-phase material.

The lattice parameters at deferent temperatures were calculated by the method of LeBail fit. Figure 3 shows the changes of the lattice constants of the doped sample as a function of temperature. As can be seen from the figure, the *a*-axis expands while the *b*-axis and the *c*-axis continuously contract as temperature increasing, which eventually cause a continuous contraction of the volume. The linear CTEs of the *a*, *b*

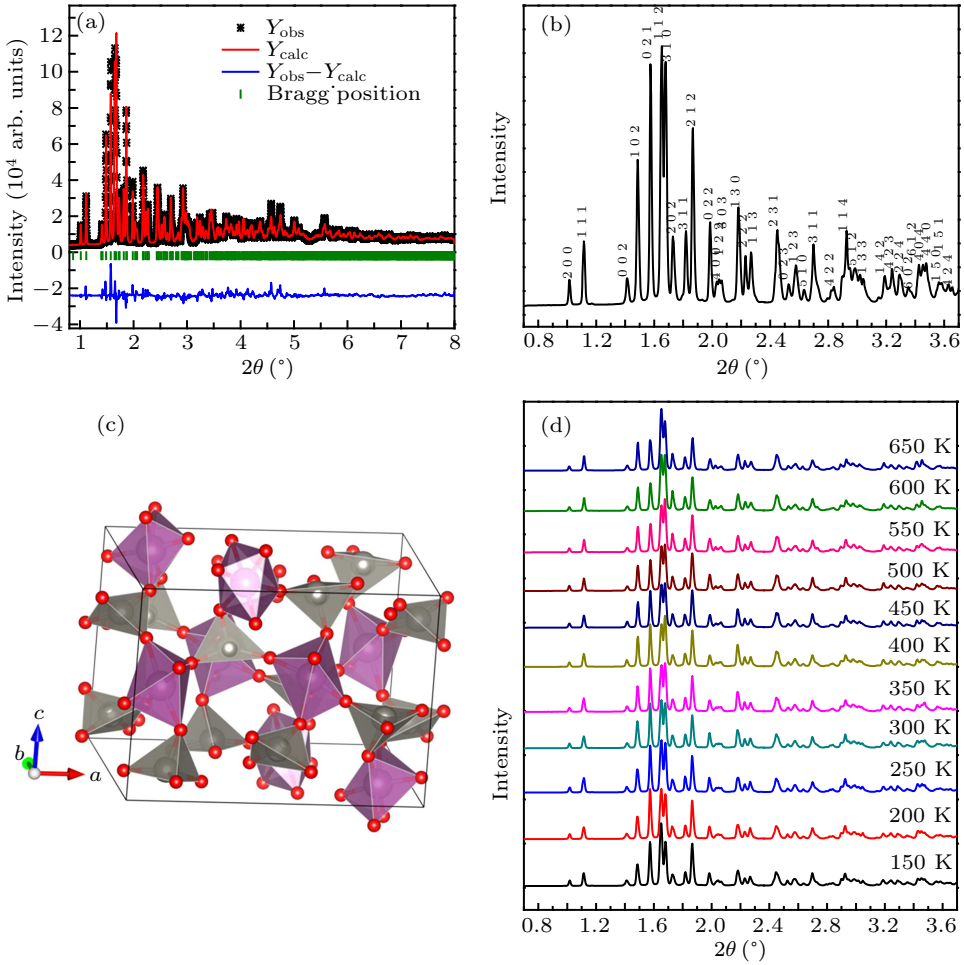


Fig. 2. (a) Results of the Rietveld refinement of the SXRD pattern at 300 K. (b) The partially enlarged SXRD pattern at 300 K with Peaks indexed. (c) Schematic diagram of the doped sample with orthorhombic symmetry depending on our experiments. O atoms are shown in red balls, ScO_6/WO_6 octahedra in purple and WO_4 tetrahedra in gray. (d) SXRD patterns of the doped sample measured from 150 K to 650 K.

Table 2. Metal atomic coordinates of the doped sample and $Sc_2(WO_4)_3$.

Atom	Sc (8d)		W1 (4c)		W2 (8d)		W3 (8d)	
$(Sc_6W_2)W_{12}O_{48\pm\delta}$	x	0.12318	x	0	x	0.14124	x	0.12318
	y	0.25644	y	0.52873	y	0.10708	y	0.25644
	z	0.46894	z	0.250	z	0.11705	z	0.46894
Occupancy	0.83746		1		1		0.16254	
$Sc_2(WO_4)_3$	x	0.46643	x	0.250	x	0.11657		
	y	0.38133	y	0	y	0.35594		
	z	0.25010	z	0.473	z	0.39454		
Occupancy	1		1		1			

and c axes in 150–650 K are calculated to be 5.64×10^{-6} K^{-1}, -3.80×10^{-6} K^{-1} and -6.33×10^{-6} K^{-1}, respectively, which results in a volumetric CTE of -4.52×10^{-6} K^{-1} and a linear CTE of -1.51×10^{-6} K^{-1}. An intrinsic NTE in the doped material is determined. This absolute value of linear CTE is a little smaller than that of the reported value -2.2×10^{-6} K^{-1} for $Sc_2W_3O_{12}$ at 10–450 K.[38] The little changes of cell parameters between the doped and undoped materials can be used to explain the little change of linear CTE.

Figure 4(a) shows the Raman spectra of the doped and undoped samples at room temperature. All the Raman modes can be identified by referring to the literature on spectroscopy studies.[3,15,39] Usually, the symmetric modes of tungstate crystal are located in the areas of the higher frequencies. Here, a strong mode centered at 1024.3 cm^{-1}, a shoulder mode near 1008.4 cm^{-1} and a weak mode near 974.1 cm^{-1} all can be assigned to the W–O symmetric stretching vibrations (ν_1) of the WO_4 tetrahedra. A weaker mode centered at 959.1 cm^{-1}, two shoulder modes near 850.3 cm^{-1} and 842.5 cm^{-1}, and a strong mode near 828.1 cm^{-1} all can be identified as the W–O asymmetric stretching vibrations (ν_3) of the WO_4 tetrahedra. The mode centered at 354.9 cm^{-1} is recognized as the antisymmetric bending vibration (ν_4) of the WO_4 tetrahedron. The modes near 327.5 cm^{-1} and 287.7 cm^{-1} are assigned to the symmetric bending vibration (ν_2) of the WO_4 tetrahedron and the rotation (T′(Sc^{3+})) of the Sc^{3+}, respectively. The mode near

258.2 cm^{-1} is considered as the rotation ($T'(Sc^{3+})$) of Sc^{3+}. The mode below 200 cm^{-1} is deemed as the translational and liberations ($T'(WO_4)$, $L(WO_4)$) of the WO_4 tetrahedra.

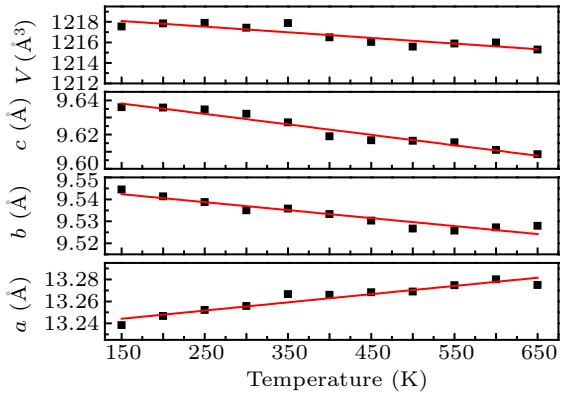


Fig. 3. The changes of the lattice constants with temperature.

Lorentz peak fitting was used to find the subtle differences between the Raman spectra of the doped and undoped samples as shown in Figs. 4(a)–4(d). Most stretching and bending modes of the doped sample are located in the positions of higher wave numbers (blueshifts) than that of $Sc_2W_3O_{12}$, indicating that the W–O bonds of the doped sample are somewhat stronger (harder) than those of $Sc_2W_3O_{12}$. This is due to the stress introduced by $W(3)^{6+}$ occupying the positions of Sc^{3+} and the distortion of the crystal. The electronegativity of Sc^{3+} (1.36) differs greatly from that of W^{6+} (2.36), which results in the significant difference of distributions of negative charges between the doped and undoped samples, and distinct changes of bond strength between the metal atom and the oxygen atom and the introduction of stress. In addition, the apparent difference of ionic radius between W^{6+} (0.41 Å) and Sc^{3+} (0.73 Å) also inevitably causes distortions of polyhedra, thus stresses are introduced. Combining it with the shrink of the unit cell volume, we can infer the stress to be compressive stress. Since the changes of bond strength and introduced stress usually cause blueshift or redshift in Raman mode frequency, the mode frequency ω_i of the doped sample can be expressed by the sum of the natural frequency $\omega_{i0}(T)$ of $Sc_2W_3O_{12}$ and the change of frequency $\Delta\omega_i$ introduced by $W(3)^{6+}$ occupying Sc^{3+} sites, that is, $\omega_i = \omega_{i0}(T) + \Delta\omega_i$.

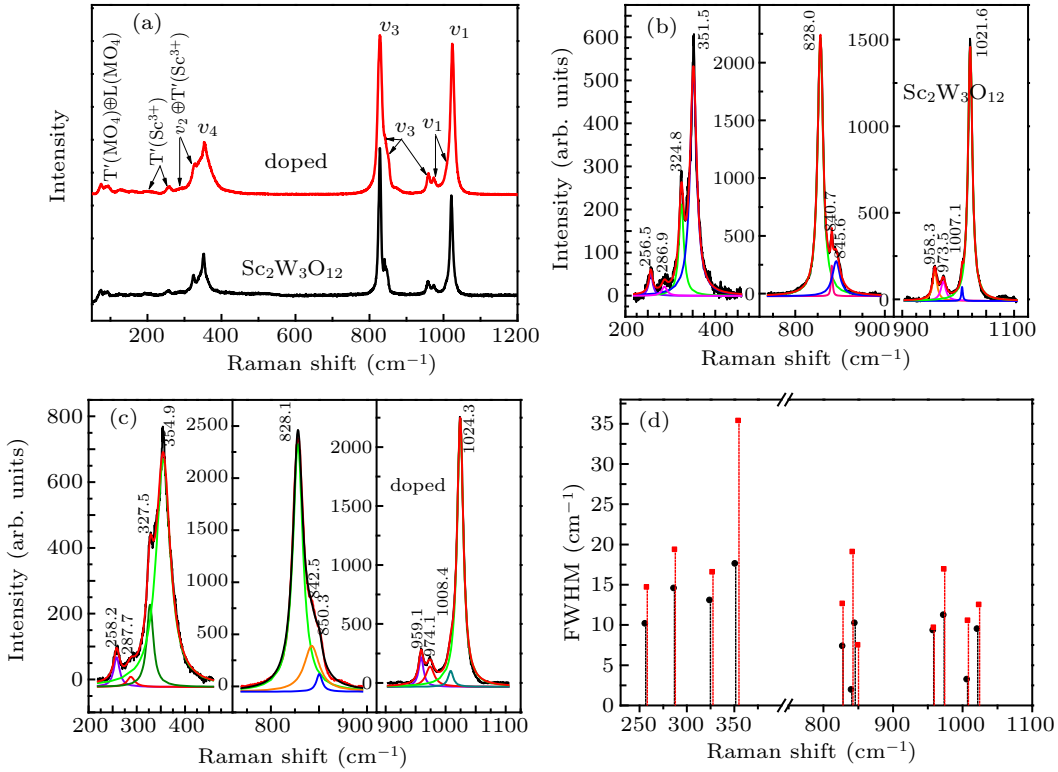


Fig. 4. (a) Raman spectra of the doped sample and $Sc_2W_3O_{12}$ at room temperature; (b)–(c) Lorentz fits of the spectra; (d) FWHMs of the Raman peaks of the spectra, squares and circles represent the data of the doped sample and $Sc_2W_3O_{12}$, respectively.

Figure 4(d) gives the comparison of full width at half maximum (FWHM) of Raman peaks of the two spectra. Obviously, the FWHMs of the doped sample are larger than that of $Sc_2W_3O_{12}$, indicating the wider linewidths of Raman peaks in the doped sample, due to the distortion of polyhedra and stress introduced. Thus the Raman linewidth, Γ, of the doped sample can be expressed by the sum of the natural linewidth, $\Gamma_0(T)$, of $Sc_2W_3O_{12}$ and the variation of linewidth $\Delta\Gamma$ caused by $W(3)^{6+}$ occupying Sc^{3+} site, namely, $\Gamma = \Gamma_0(T) + \Delta\Gamma$.

Structure stability of different Sc^{3+} occupied by W^{6+} in the unit cell of $Sc_2W_3O_{12}$ was analyzed by first-principles calculations based on DFT. Results show that with one W^{6+} occupying the site of Sc^{3+}, the polyhedron distorted severely and the structure of crystal is unstable (substitutional energy

1.19 eV/W, the positive value implies that the substitution is endothermal). The unit cell parameters of the crystal are as follows: $a = 13.22$ Å, $b = 9.61$ Å, $c = 9.96$ Å. It no longer maintains the orthorhombic structure ($\alpha = 91°$, $\beta = 93°$, $\gamma = 89°$). With two W^{6+} occupying the sites of Sc^{3+}, the structure of crystal is more stable than the former case (substitutional energy 0.85 eV/W). The unit cell parameters of the crystal are as follows: $a = 13.56$ Å, $b = 9.66$ Å, $c = 9.79$ Å. The orthorhombic structure is still maintained. Compared to the unit cell parameters of the undoped sample ($a = 13.66$ Å, $b = 9.72$ Å, $c = 9.83$ Å), the volume of the doped crystal shrinks lightly. Figures 5(a)–5(c) give the schematic diagrams of $Sc_2W_3O_{12}$ crystal and the crystals with different Sc^{3+} occupied by W^{6+}. These calculation results further demonstrate the reliability of the structure of the doped sample.

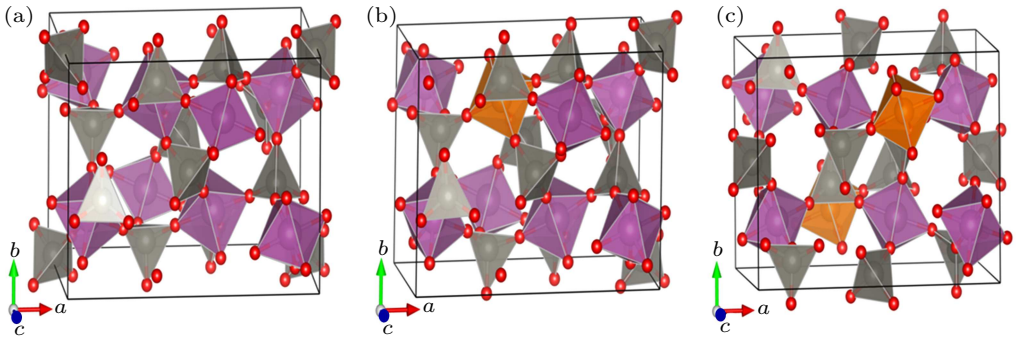


Fig. 5. (a) Schematic diagram of the $Sc_2W_3O_{12}$ crystal. (b) Schematic diagram with one W occupying Sc site in the unit cell of $Sc_2W_3O_{12}$. (c) Schematic diagram with two W occupying Sc sites in the unit cell of $Sc_2W_3O_{12}$. O atoms are shown in red balls, ScO_6 octahedra in purple, WO_6 octahedrain in brown and WO_4 tetrahedra in gray.

4. Conclusions

In summary, we have investigated the effects of W^{6+} occupying the sites of Sc^{3+} in the unit cell of $Sc_2W_3O_{12}$ by employing experiment and first-principles calculations. The structure of the doped sample $(Sc_6W_2)W_{12}O_{48\pm\delta}$ is similar to that of orthorhombic $Sc_2W_3O_{12}$ but with three unequivalent W in the sites of the crystal lattice, two of which occupy the positions similar to $Sc_2W_3O_{12}$, and the other one occupies the remaining positions of Sc and thus formed WO_6 octahedra. It also exhibits an intrinsic NTE property (linear CTE, -1.51×10^{-6} K^{-1}) within the measured temperature range (150 K–650 K). Compared to the Raman spectrum of $Sc_2W_3O_{12}$, the stretching modes and bending modes of the doped samples shift toward the higher wave numbers, indicating that the W–O bonds in the doped sample become harder (stronger). In addition, the increase of the FWHMs means the broadening of Raman linewidths in the spectrum of the doped sample. The distortion of crystal and stress in crystal, induced by W^{6+} occupying Sc^{3+}, are account for these changes. Results of first-principles calculations show that the crystal with even W^{6+} occupying even Sc^{3+} in the unit cell is stable while the structure with odd W^{6+} occupying odd Sc^{3+} in the unit cell is unstable due to the unit cell is severely distorted. It further proves the reliability of the structure of the doped sample.

References

[1] Mary T A, Evans J S O, Vogt T and Sleight A W 1996 *Science* **272** 90
[2] Turquat C, Muller C, Nigrelli E, Leroux C and Nihoul G 2000 *Eur. Phys. J. AP* **10** 15
[3] Maczka M, Hermanowicz K and Hanuza J 2005 *J. Mol. Struct.* **744–747** 283
[4] Liu Q, Fan C, Wu G, Zhao Y, Sun X, Cheng X, Shen J and Hu Y 2015 *Ceram. Int.* **41** 8267
[5] Liu Q Q, Cheng X N and Yang J 2012 *Mater. Technol.* **27** 388
[6] Tyagi A K, Achary S N and Mathews M D 2002 *J. Alloys Compd.* **339** 207
[7] Sleight A W and Brixner L H 1973 *J. Solid State Chem.* **7** 172
[8] Sumithra S and Umarji A M 2004 *Solid State Sci.* **6** 1313
[9] Marinkovic B A, Jardim P M, de Avillez R R and Rizzo F 2005 *Solid State Sci.* **7** 1377
[10] Sumithra S and Umarji A M 2005 *Mater. Res. Bull.* **40** 167
[11] Miller K J, Romao C P, Bieringer M, Marinkovic B A, Prisco L and White M A 2013 *J. Am. Ceram. Soc.* **96** 561
[12] Liu X, Cheng Y, Liang E and Chao M 2014 *Phys. Chem. Chem. Phys.* **16** 12848
[13] Li Z, Song W and Liang E 2011 *J. Phys. Chem. C* **115** 17806
[14] Li F, Liu X, Song W, Yuan B, Cheng Y, Yuan H, Cheng F, Chao M and liang E 2014 *J. Solid State Chem.* **218** 15
[15] Hanuza J, Maczka M, Hermanowicz K, Andruszkiewicz M, Pietraszko A, Strek W and Dereń P 1993 *J. Solid State Chem.* **105** 49
[16] Ge X, Mao Y, Li L, Li L, Yuan N, Cheng Y, Guo J, Chao M and Liang E 2016 *Chin. Phys. Lett.* **33** 046503
[17] Ari M, Jardim P M, Marinkovic B A, Rizzo F and Ferreira F F 2008 *J. Solid State Chem.* **181** 1472
[18] Song W B, Wang J Q, Li Z Y, Liu X S, Yuan B H and Liang E J 2014 *Chin. Phys. B* **23** 066501
[19] Wu M M, Xiao X L, Hu Z B, Liu Y T and Chen D F 2009 *Solid State Sci.* **11** 325
[20] Chen J, Xing X, Yu R and Liu G 2005 *J. Am. Ceram. Soc.* **88** 1356
[21] Sun C, Cao Z, Chen J, Yu R, Sun X, Hu P, Liu G and Xing X 2008 *Phys. Status Solidi* **245** 2520
[22] Chen J, Xing X R, Liu G R, Li J H and Liu Y T 2006 *Appl. Phys. Lett.* **89** 101914
[23] Sun Y, Wang C, Wen Y, Zhu K and Zhao J 2007 *Appl. Phys. Lett.* **91** 231913
[24] Takenaka K, Asano K, Misawa M and Takagi H 2008 *Appl. Phys. Lett.* **92** 011927
[25] Wang C, Sun Y, Wen Y C, Chu L H and Nie M 2010 *Mater. Sci. Forum* **638–642** 2195
[26] Wang X, Huang Q, Deng J, Yu R, Chen J and Xing X 2011 *Inorg. Chem.* **50** 2685
[27] Sebastian L, Sumithra S, Manjanna J, Umarji A M and Gopalakrishnan J 2003 *Mater. Sci. Eng. B* **103** 289

[28] Fallon G D and Gatehouse B M 1982 *J. Solid State Chem.* **44** 156
[29] Naruke H and Yamase T 2003 *J. Solid State Chem.* **173** 407
[30] Shi N, Sanson A, Gao Q, Sun Q and Chen J 2020 *J. Am. Chem. Soc.* **142** 3088
[31] Shi N, Gao Q, Sanson A, Li Q, Fan L, Ren Y, Olivi L, Chen J and Xing X 2019 *Dalton Trans.* **48** 3658
[32] Wang C, Chang D, Gao Q, Liu C, Wang Q, Huang X and Jia Y 2020 *Phys. Chem. Chem. Phys.* **22** 18655
[33] Gao Q, Sun Y, Shi N, Milazzo R and Chen J 2020 *Scr. Mater.* **187** 119
[34] Chen J, Gao Q, Sun Q, Chang D, Huang Q, Wu H, Sanson A, Milazzo R, Zhu H and Li Q 2017 *Angew. Chem.* **129** 9031
[35] Kresse G and Furthmüller J 1996 *Phys. Rev. B* **54** 11169
[36] Kresse G, Joubert D 1999 *Phys. Rev. B* **59** 1758
[37] Perdew J, Burke K and Ernzerhof M 1996 *Phys. Rev. Lett.* **77** 3865
[38] Evans J, Mary T and Sleight A 1998 *J. Solid State Chem.* **137** 148
[39] Paraguassu W, Maczka M, Filho A G S, Freire P T C, Melo F E A, Filho J M and Hanuza J 2007 *Vib. Spectrosc.* **44** 69